A Power-Series Buildup Factor Formulation. Application to Rectangular and Off-Axis Disk Source Problems*

J. H. Hubbell

(May 31, 1963)

The response (e.g., dose-rate) of an isotropic detector to primary radiation from a finite plane source may, for points less than a mean-free-path distant, be evaluated as the sum over an infinite series, This series is derived by expanding the exponential dependence $\exp(-\mu_0 r)$ as a power series in $\mu_0 r$ and integrating, numerically or analytically, each term over the source array. If the medium is effectively infinite and homogeneous, the scattering properties of this medium can be characterized by a point isotropic source buildup factor. Buildup factor data are often approximated by formulas having simple analytic dependences on $\mu_0 r$ and numerical parameters independent of $\mu_0 r$. Any such set of parameters can be used to generate a set of weight functions b_n for an infinite series buildup factor representation

$$\exp(+\mu_0 r) \sum_{n=0}^{\infty} b_n \cdot (-\mu_0 r)^n / n!$$

which can be used with the above primary radiation series solution to give, instead, a series solution including both primary and scattered radiation. Tables of b_n's (air-dose buildup only) derived from coefficients of cubic polynomials fitted to the Goldstein-Wilkins data (NYO–3075) are given for $0 \leq n \leq 13$ at primary photon energies of 0.5, 0.7, 1.0, 1.5, 2.0, 3.5, 5.5, 7.5, and 9.5 Mev in water, Al, Fe, Sn, W, Pb, and U. The method is applied to give: (1) a comparison with dose-rates measured by a detector separated from a Co-60 rectangular plaque food irradiator by a layer of steel and a layer of water and (2) dose-rate profiles at constant heights across a cleared circular area in a Co-60 infinite plane source in air.

1. Introduction

A number of methods for evaluating radiation fields from distributed sources have been developed as part of a general program at the National Bureau of Standards [1, 2][1] and other agencies. Some of these methods, which provide easy and rapid solutions to radiation shielding problems, rely on the approximate proportionality between dose-rate and the solid angle subtended by a uniformly radiating surface. This approximation has been shown to be quite good if the material interposed between source and detector is of the order of a mean free path in thickness [3].

For situations involving much less than a mean free path of interposed material, as in the case of a detector separated from a surface deposition of radioactive material by only a thin roof or a few feet of air [4, 5], the power-series method developed by Sievert [6] for circular disk sources has been extended [7, 8] to include rectangular sources and to take into account point-source buildup factor data in polynomial form [9].

In addition, it has been reported [10] that buildup data from a number of other analytic formulations [11–15] can also readily be transformed for direct use in a Sievert-type power-series solution. The present work constitutes a published account of the material reported in [10] and includes a quantitative comparison of the buildup data formulations considered [9, 11–15] for Co-60 gamma rays in aluminum for zero to ten mean-free-path penetrations, a table of buildup data transformations, a sample table of transformed buildup data, and sample calculations and results.

Besides fallout radiation studies [5], the power series method is applicable, or has already been applied [16] to such diverse distributed source studies as:

(a) Tracer studies involving an elongated rectangle as the initial distribution of radioisotope-tagged sand in a beach-erosion sand-drift experiment [16],

(b) food irradiator design studies involving plaque sources [3, 17, 18], and

(c) calculation of the dose distribution in tissue adjacent to disk or other shaped radioactive applicators for treatment of malignancies [6, 19]. Also, buildup data in the form of the series coefficients presented here are directly applicable to a method

of barrier shape optimization described by Jain and Sharma [20] who use, in effect, the first three terms of this series for their analysis.

2. Buildup Factor: Definition and Discussion

As in references [9] through [15], the source and detector environment is idealized throughout this paper as a homogeneous infinite medium, shown schematically in figure 1. In such an idealized situation the scattered radiation reaching the detector can be taken into account by means of a point isotropic (PTI) source buildup factor [21]

$$B_{\text{PTI}}(E_0, Z, r) = (D^0 + D^s)/D^0 \qquad (1)$$

which depends on the effective atomic number Z characterizing the medium and the distance r between the detector and a monoenergetic point source of photons of energy [2] E_0.

The quantities D^0 and D^s in (1) refer to the unscattered and the scattered components, respectively, of the radiation received by the detector. For a given physical situation, D^0 and D^s (and hence $B_{\text{PTI}}(E_0, Z, r)$) can assume a variety of numerical values depending on what kind of detector response (e.g., photon number flux [22], energy current [22] at an interface, energy dissipation in a medium- or air-equivalent detector, etc.) is used to describe the radiation field. The buildup factor data in this work correspond to a detector which measures radiation *flux* in terms of *energy dissipation in air*. In this case $B_{\text{PTI}}(E_0, Z, r)$, D^0 and D^s in (1) are the same as the quantities B_d, $I_d^{(0)}$ and $I_d^{(s)}$ defined in [21].

---

[2] Here, and in what follows, the source is considered to be either monoenergetic or an effectively monoenergetic component of a photon energy distribution over which the final results must be summed.
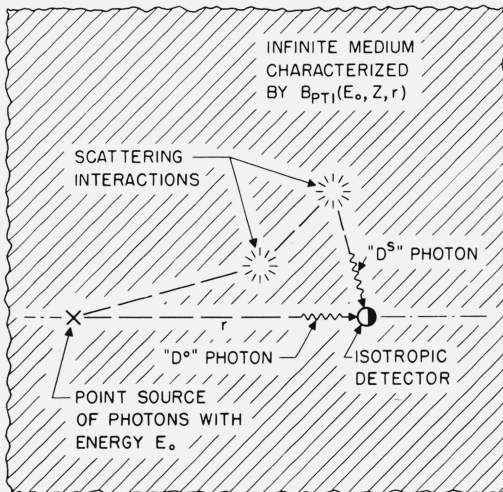
The total detector response D to a point isotropic source is

$$D = D^0 + D^s = D^0 B_{\text{PTI}}(E_0, Z, r)$$
$$= (k/4\pi)[\exp(-\mu_0 r)/r^2] B_{\text{PTI}}(E_0, Z, r) \qquad (2)$$

in which $\mu_0 [=\mu(E_0, Z)]$ is the narrow-beam attenuation coefficient [23] at photon energy E_0 for the *medium*. The source strength factor k, for the detector response-type $(D = I_d)$ specified above is

$$k = n \times E_0 \times \mu_{en}(E_0, Z) \times (\text{dimensional factors}) \qquad (3)$$

where n is the total number of photons of energy E_0 emitted per second by the source, $\mu_{en}(E_0, Z)$ is the energy absorption coefficient [24] for *air*,[3] and the "dimensional factors" provide the units [e.g., (rads/hr)/curie] desired in the final answer.

3. Analytic Formulations for $B_{\text{PTI}}(E_0, Z, r)$

For applying buildup data to distributed source problems, the dependence of $B_{\text{PTI}}(E_0, Z, r)$ on r is usually approximated by some analytic function. This not only provides some economy in data tabulation, but the function can be so chosen that its presence entails little or no additional complication in the integration

$$D = (\sigma/4\pi) \int_S [\exp(-\mu_0 r)/r^2] B_{\text{PTI}}(E_0, Z, r) dS \qquad (4)$$

of (2) over a distributed source S with differential elements dS, as schematized in figure 2. The constant factor in (4)

$$\sigma = dk/dS \qquad (5)$$

---

[3] Note, however, that example 1 in section 7 requires an answer in terms of energy dissipation in *water* $(D = I_D)$ rather than in *air* $(D = I_d)$, so, that $\mu_{en}(E_0, H_2O)$ is used in the computation in 7.1, rather than $\mu_{en}(E_0, \text{air})$ corresponding to the data in table 3 in section 5.

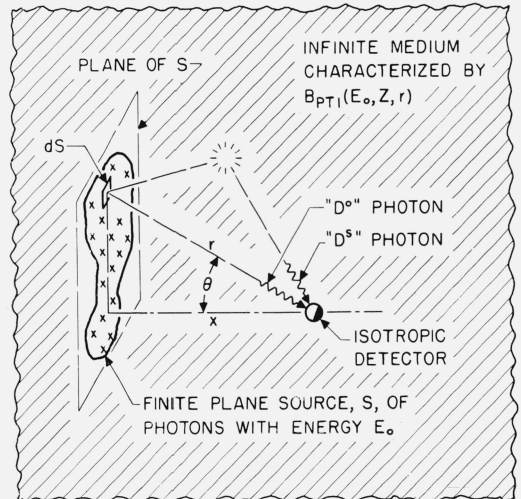FIGURE 1. *Point isotropic source geometry.*

FIGURE 2. *Finite plane isotropic source geometry.*

is the source strength per unit of source area or volume, with k defined as in (3).

The following functions (a) to (f) have been used to represent point isotropic source $B_{PTI}(E_0, Z, r)$ data in order to obtain analytic solutions to (4).

(a) Linear approximation [11] (one parameter):

$$B_{PTI}(E_0, Z, r) = 1 + a\mu_0 r \qquad (6)$$

where

$$a = (\mu_0 - \mu_{en})/\mu_{en}. \qquad (7)$$

(b) Exponential-linear empirical fit [12] (two parameters):

$$B_{PTI}(E_0, Z, r) = 1 + a\mu_0 r \exp(-b\mu_0 r). \qquad (8)$$

(c) Exponential-polynomial fit [13] (one or three parameters):

$$B_{PTI}(E_0, Z, r) = \exp(+\mu_0 r)(br + 1) \qquad (9a)$$

or, for larger thicknesses:

$$B_{PTI}(E_0, Z, r) = \exp(+\mu_0 r)(ar^2 + br + c). \qquad (9b)$$

(d) Low order polynomial fit [9, 25] (three parameters):

$$B_{PTI}(E_0, Z, r) = 1 + \beta_1 \mu_0 r + \beta_2 (\mu_0 r)^2 + \beta_3 (\mu_0 r)^3. \qquad (10)$$

(e) Sum-of-exponentials fit [14] (three parameters):

$$B_{PTI}(E_0, Z, r) = A \exp(-a_1 \mu_0 r) + (1-A) \exp(-a_2 \mu_0 r) \qquad (11)$$

(f) Exponential-linear moments calculation result [15] (four parameters):

$$B_{PTI}(E_0, Z, r) = 1 + \mu_0 r \{ A_1 B_1 \exp[(1-B_1)\mu_0 r]$$
$$+ A_2 B_2 \exp[(1-B_2)\mu_0 r] \}. \qquad (12)$$

Table 1 contains data calculated at $\mu_0 r = 1, 2, 4, 7,$ and 10 mean free paths according to approximation (a) above, empirical fits (b) to (e) and direct-result parameters (f), in addition to earlier calculated results from NYO–3075, [26] (g), all for "exposure dose" (air-equivalent detector) in aluminum and interpolated to 1.25 Mev.

The column headed ϵ_f beside each column of calculated data contains percent deviations from the recent Berger-Spencer [15] results (f),

$$\epsilon_f = \frac{B - B \text{ (Berger-Spencer)}}{B \text{ (Berger-Spencer)}} \times 100\% \qquad (13)$$

and the column headed ϵ_g contains percent deviations from the Goldstein-Wilkins results (g) to which (b), (d), and (e) were fitted,

$$\epsilon_g = \frac{B - B \text{ (Goldstein-Wilkins)}}{B \text{ (Goldstein-Wilkins)}} \times 100\%. \qquad (14)$$

As seen in table 1, the Goldstein [11] linear approximation (a), above, involves neither fitting nor transport theory calculations. It is very useful for penetrations up to one or two mean free paths, and gives results within a factor of two up to ten mean free paths in aluminum.

TABLE 1. *The point isotropic source buildup factor ("exposure dose": air-equivalent detector), $B_{PTI}(E_0, Z)$, for 1.25-Mev gamma rays in aluminum evaluated from five different analytic approximations (a to e) at 0, 1, 2, 4, 7, and 10 mfp, compared with the corresponding moments-calculated analytic (f) and numerical (g) results*

$\mu_0 r$	(a) Goldstein [11] 1-parameter linear approximation (6)			(b) Chilton et al. [12] 2-parameter exponential-linear fit (8)			(c) Leshchinskii [13] 1-parameter exponential-linear fit (9a)		
	B_{PTI}	ϵ_f*	ϵ_g**	B_{PTI}	ϵ_f	ϵ_g	B_{PTI}	ϵ_f	ϵ_g
		%	%		%	%		%	%
0	1.00	0	0	1.00	0	0	1.00	0	0
1	2.06	7.9	7.3	1.97	3.1	2.6	1.80	−5.8	−6.3
2	3.01	−1.0	−2.0	3.06	0.7	−0.3	2.41	−21	−21
4	5.04	−13	−13	5.69	−2.2	−2.2	−18.9		
7	8.04	−27	−29	11.0	0	−3.5	−1490		
10	11.0	−36	−37	18.3	6.4	4.6	−52100		

$\mu_0 r$	(d) Capo [9] 3-parameter polynomial (cubic) fit (10)			(e) Taylor [14] 3-parameter sum-of-exponnetials fit (11); Lakey [28] data			(f) Berger-Spencer [15] 4-parameter exponential-linear moments calculation results (12)	(g) Goldstein-Wilkins [26] moments calculation results; Al data in tabulated form only
	B_{PTI}	ϵ_f	ϵ_g	B_{PTI}	ϵ_f	ϵ_g	B_{PTI}	B_{PTI}
		%	%		%	%		
0	0.997	−0.3	−0.3	1.00	0	0	1.00	1.00
1	1.93	1.0	0.5	2.10	9.0	9.4	1.91	1.92
2	3.05	0.3	−0.7	3.26	7.2	6.2	3.04	3.07
4	5.81	−0.2	−0.2	5.76	−1.0	−1.0	5.82	5.82
7	11.1	0.9	−2.6	10.2	−7.3	−11	11.0	11.4
10	17.6	2.3	0.6	15.7	−8.7	−10	17.2	17.5

* $\epsilon_f = \{[B_{PTI} - B_{PTI}(\text{Berger-Spencer})]/B_{PTI}(\text{Berger-Spencer})\} \times 100\%$.
** $\epsilon_g = \{[B_{PTI} - B_{PTI}(\text{Goldstein-Wilkins})]/B_{PTI}(\text{Goldstein-Wilkins})\} \times 100\%$.

The two-parameter exponential-linear empirical fit (b) of Chilton, Holoviak, and Donovan [12] is surprisingly good for penetrations up to ten mean free paths. This formulation, similar in form to the calculated result (f) of Berger and Spencer [15], can thus provide economical storage and easy application of buildup data over a wider range of penetration thicknesses. Reference [12] contains parametric data for aluminum only, which was the deciding factor in selecting this as the reference substance for table 1.

Leshchinskii [13] supplied data, for the reference situation of Co–60 gammas in aluminum, only for the one-parameter exponential-linear fit (9a), intended for penetrations of 0 to 10 cm (0 to 1.49 mean free paths), although for Co–60 gammas in water he *did* use the three-parameter fit (9b) for penetrations of 2 to 70 cm (0.127 to 4.44 mean free paths). In each case the fit is within about 5 percent up to the specified upper limit and then departs wildly. However, this formulation does have the advantage that the exponential dependence $\exp(-\mu_0 r)$ is canceled out of the distributed source integral (4), and it will be seen that the power-series solution of (4) [8, 10] is, in effect, a generalization of the Leshchinskii result.

The slight departure of the Capo data (d) from the condition $B_{\mathrm{PTI}}(E_0,\ Z,\ r)=1$ at $\mu_0 r=0$ results from additional cross fitting as a polynomial in energy or reciprocal energy, in which it is difficult to preserve this normalization. This discrepancy is not large enough to detract from the usefulness of the data, however, and in this specific comparison (1.25 Mev photons in Al) the departures ϵ_f and ϵ_g from calculated data (f) and (g) are seen to be less, over the given range of $\mu_0 r$ values, than corresponding departures of (a), (b), (c), and (e).

In addition to the empirically fitted Capo tabulation, β_i polynomial coefficients for Co–60 and Cs–137 gamma rays in concrete and water were directly calculated by Spencer [1] using the moments method and were punched on IBM cards for use in further calculations. In [1] the A_j coefficients in (A1), page 80, are identical with β_i coefficients if (a) A_j refers to the zeroth Legendre harmonic ($l=0$), and (b) A_j refers to integral dose data rather than to the differential energy data indicated by the dependence on E_i in (A1).

The sum-of-exponentials three-parameter fit (4) of Taylor [14] is perhaps the most well-known and widely used buildup factor formulation in current use [27]. The only published parametric data for aluminum seem to be those of Lakey [28], and these were used for the comparison in table 1.

The exponential-linear four-parameter formula (f) of Berger and Spencer [15] represents direct calculated results by the moment method [21]. Parametric data in [15] are tabulated for 0.0341- to 10.22-Mev gamma-rays in aluminum and concrete, and additional formulas are supplied for applying these buildup parameters to such geometries as the isotropic disk source (on-axis) and the isotropic spherical surface source. The buildup data in table 1, obtained by evaluating (12) using parameters interpolated to 1.25 Mev, agree within 4 percent with the earlier moments calculation [21] results of Goldstein and Wilkins [26], (g), to which the formulas (b), (d), and (e) were fitted.

4. Power-Series Solution for Unscattered Radiation From a Distributed Source

It has been shown [6, 7] that for finite plane sources of simple shape, a solution of (4) for D^0 (i.e., omitting the factor $B_{\mathrm{PTI}}(E_0,\ Z,\ r)$ within the integrand) may be obtained in the form of an infinite series

$$D^0=(\sigma/4\pi)\sum_{n=0}^{\infty} q_n(\text{geom})\cdot(\mu_0 x)^n \qquad (15)$$

which converges quickly when the detector is less than a mean free path from the source. The dimensionless $q_n(\text{geom})$ coefficients in (15) depend only on the *shape* of the detector-source geometry, and are derived from a power series expansion of the exponential in (4)

$$\exp(-\mu_0 r)=\sum_{n=0}^{\infty}(-\mu_0 r)^n/n! \qquad (16)$$

such that

$$q_n(\text{geom})=\int_S(-r/x)^n dS/(r^2\cdot n!). \qquad (17)$$

The quantity $\mu_0 x$, also dimensionless, is the mean-free-path thickness of material between source and detector.

Formulas and tables of $q_n(\text{geom})$ coefficients (tables include values for $0\leq n\leq 9$) have been generated for a rectangular source [7] and for a circular disk source with detector off-axis [8]. As a check, it was noted [8] that for a detector on-axis over a circular disk source the series (15) reduces to the familiar exponential-integral solution, in which the exponential integrals $E_1(x)$ are replaced by power series in x.

5. Adaptation of Analytic $B_{\mathrm{PTI}}(E_0,\ Z,\ r)$ Formulations to the Distributed Source Power-Series Solution

In the series solution (15) for the unscattered component D^0 in section 4, the material between source and detector can either be distributed throughout the intervening space, or can be arranged as one or more uniform slabs or sheets lying parallel to the source-plane. In this section, on the other hand, the source and detector are assumed embedded, as discussed in section 2, in an infinite homogeneous medium.

Replacing the polynomial in the Leshchinskii formula (9b) by a power series we obtain the buildup factor formulation

$$B_{\mathrm{PTI}}(E_0, Z, r) = \exp\ (+\mu_0 r) \sum_{n=0}^{\infty} b_n(E_0, Z) \cdot (-\mu_0 r)^n / n! \tag{18}$$

reported in [10], from which the coefficients [4] $b_n(E_0, Z)$ can be used with the series solution (15). The only change in (15) is the multiplication of each series term $q_n(\mathrm{geom}) \cdot (\mu_0 x)^n$ by the additional factor $b_n(E_0, Z)$ to give the *total* dose-rate solution

$$D = D^0 + D^S = (\sigma/4\pi) \sum_{n=0}^{\infty} b_n(E_0, Z) \cdot q_n(\mathrm{geom}) \cdot (\mu_0 x)^n. \tag{19}$$

Equations (18) and (19) are, of course, of little practical value if an infinite number of $b_n(E_0, Z)$ coefficients must be fitted and tabulated. However, by expanding as power-series all exponentials appearing in the analytic formulations (a) to (f) in section 3, then equating coefficients of like powers of $\mu_0 r$, a transformation for generating $b_n(E_0, Z)$ coefficients from the parameters of any of these formulations may be obtained. Table 2 presents these "parasite" transformations, and includes (18) for comparison.

---

[4] The simpler notation $b_n(E_0, Z)$, used throughout this work, is equivalent to $B'_n(E_0, Z)$ used in [8] and [10].

The surprisingly simple transformation (e) of Taylor [14] and Lakey [28] parametric data results because inclusion of a $B_{\mathrm{PTI}}(E_0, Z, r)$ of this form into (4) produces no change in the analytic form of the integrand. It can also be seen in table 2 that the Goldstein [11] linear approximation (a) is a special case of the polynomial fit (d) used by Capo [9], and that the four-parameter calculated result (f) of Berger and Spencer [15] is identical in analytic form with the two-parameter empirical fit (b) of Chilton et al. [12]. The similarities are reflected in the respective transformations in the last column.

To illustrate the use of table 2, transformation (d) was used to generate the $b_n(E_0, Z)$ values for $0 \leq n \leq 13$ in table 3 from "dose" (air-equivalent detector) buildup data for water, Al, Fe, Sn, Pb, W, and U in the form of $\beta_i(E_0, Z)$ polynomial coefficients. The input $\beta_i(E_0, Z)$'s were taken from reference [9], tables 1B, 4B, 7B, 10C, 13B, 16C, and 18B which in turn were fitted by least squares to data calculated by Goldstein and Wilkins [26] using the moments method. Of the 15 gamma-ray energies from 0.4 to 9.5 Mev presented in [9] for reactor "operating" and "shutdown" shielding calculations, the 10 energies $E_0 = 0.5$, 0.7, 1.0, 1.5, 2.0, 2.5, 3.5, 5.5, 7.5, and 9.5 Mev were arbitrarily selected.

The appearance in table 3 of $b_0(E_0, Z)$ $\{= \beta_0(E_0, Z) = B(E_0, Z, r)$ at $\mu_0 r = 0\}$ values which are not unity follows from the discussion of the Capo data in section 3.

TABLE 2.—*Summary of analytic formulations (a to f) for the point isotropic source buildup factor $B_{\mathrm{PTI}}(E_0, Z)$ (column 4)*

The power-series formulation, in which the "∞" for number of parameters (column 3) may be replaced by 1, 2, 3, 4, or N, depending on which of the formulations (a to f) is used for generating the $b_n(E_0, Z)$ coefficients, has been added for comparison. The last column contains the "parasite" transformations, of which (d) was used to generate the sample $b_n(E_0, Z)$'s in table 3 from the Capo [9] tables of β_i polynomial coefficients

Formulation	Reference	Number of parameters	$B_{\mathrm{PTI}}(E_0, Z, r)$, point isotropic source	Eq No.	$b_n(E_0, Z)$; $n = 0, 1, 2, \ldots$
(a)	Goldstein [11]	1	$1 + a\mu_0 r$	(6)	$1 - na$
(b)	Chilton, Holoviak, Donovan [12]	2	$1 + a\mu_0 r \exp(-b\mu_0 r)$	(8)	$1 - a \sum_{i=1}^{n} i \binom{n}{i} b^{i-1}$
(c)	Leshchinskii [13]	1	$\exp(+\mu_0 r)(br + 1)$	(9a)	$b_0 = 1; b_1 = -b/\mu_0; b_{n \geq 2} = 0$
		3	$\exp(+\mu_0 r)(ar^2 + br + c)$	(9b)	$b_0 = c; b_1 = -b/\mu_0; b_2 = 2a/\mu_0^2; b_{n \geq 3} = 0$
(d)	Capo [9]	3 or N	$\sum_{i=0}^{N} \beta_i(E_0, Z)(\mu_0 r)^i$	(10)	$\sum_{i=0}^{n \leq N} (-1)^i \{n! / (n-i)!\} \beta_i(E_0, Z)$
(e)	Taylor, [14] Lakey [28]	3	$A \exp(-a_1\mu_0 r) + (1 - A) \exp(-a_2\mu_0 r)$	(11)	$A(1 + a_1)^n + (1 - A)(1 + a_2)^n$
(f)	Berger, Spencer [15]	4	$1 + \mu_0 r\{A_1 B_1 \exp[-(B_1 - 1)\mu_0 r] + A_2 B_2 \exp[-(B_2 - 1)\mu_0 r]\}$	(12)	$1 - \sum_{i=1}^{n} i \binom{n}{i} \{A_1 B_1 (B_1 - 1)^{i-1} + A_2 B_2 (B_2 - 1)^{i-1}\}$
Power series	This work	∞	$\exp(+\mu_0 r) \sum_{n=0}^{\infty} b_n(E_0, Z) \cdot (-\mu_0 r)^n / n!$	(18)	$b_n(E_0, Z)$

TABLE 3. *Coefficients $b_n(E_0, Z)$ of the power-series buildup factor formulation (18) derived from the Capo [9] β_i polynomial coefficients according to transformation (d), table 2.

These b_n (E_0, Z) coefficients may be used directly in the distributed source series solution (19) with geometry coefficeints q_n (geom) (17) such as are given in references [7] and [8] for rectangular or off-axis disk sources.

			$b_n(E_0, H_2O)$		
n \ E_0(Mev)	0.5	0.7	1.0	1.5	2.0
0	1.0011 (0)	1.0008 (0)	9.9678 (−1)	9.9480 (−1)	9.9542 (−1)
1	6.4656 (−2)	5.0643 (−2)	9.7950 (−3)	6.6752 (−2)	1.5973 (−1)
2	2.3708 (−1)	−2.4382 (−1)	−6.3441 (−1)	−7.1188 (−1)	−5.9935 (−1)
3	1.4491 (0)	1.0713 (−1)	−9.2998 (−1)	−1.3348 (0)	−1.2776 (0)
4	3.6313 (0)	1.0932 (0)	−8.7105 (−1)	−1.7959 (0)	−1.8709 (0)
5	6.7143 (0)	2.7040 (0)	−4.5177 (−1)	−2.0887 (0)	−2.3751 (0)
6	1.0629 (1)	4.9293 (0)	1.3372 (−1)	−2.2071 (0)	−2.7859 (0)
7	1.5306 (1)	7.7588 (0)	3.4913 (0)	−2.1448 (0)	−3.0992 (0)
8	2.0675 (1)	1.1182 (1)	3.0268 (0)	−1.8955 (0)	−3.3109 (0)
9	2.6668 (1)	1.5189 (1)	4.9461 (0)	−1.4529 (0)	−3.4167 (0)
10	3.3216 (1)	1.9769 (1)	7.2551 (0)	−8.1092 (−1)	−3.4124 (0)
11	4.0248 (1)	2.4912 (1)	9.9595 (0)	3.6838 (−2)	−3.2940 (0)
12	4.7695 (1)	3.0608 (1)	1.3065 (1)	1.0966 (0)	−3.0571 (1)
13	5.5489 (1)	3.6846 (1)	1.6578 (1)	2.3746 (0)	−2.6977 (0)

n \ E_0(Mev)	2.5	3.5	5.5	7.5	9.5
0	9.9663 (−1)	9.9899 (−1)	1.0022 (0)	1.0042 (0)	1.0054 (0)
1	2.4502 (−1)	3.7542 (−1)	5.2925 (−1)	6.1392 (−1)	6.6696 (−1)
2	−4.6449 (−1)	−2.3628 (−1)	4.9890 (−2)	2.1199 (−1)	3.1471 (−1)
3	−1.1293 (0)	−8.3515 (−1)	−4.3613 (−1)	−2.0236 (−1)	−5.2252 (−2)
4	−1.7467 (0)	−1.4203 (0)	−9.2912 (−1)	−6.2983 (−1)	−4.3481 (−1)
5	−2.3140 (0)	−1.9906 (0)	−1.4294 (0)	−1.0711 (0)	−8.3385 (−1)
6	−2.8287 (0)	−2.5453 (0)	−1.9372 (0)	−1.5270 (0)	−1.2503 (0)
7	−3.2881 (0)	−3.0834 (0)	−2.4529 (0)	−1.9981 (0)	−1.6849 (0)
8	−3.6895 (0)	−3.6040 (0)	−2.9767 (0)	−2.4851 (0)	−2.1387 (0)
9	−4.0302 (0)	−4.1060 (0)	−3.5090 (0)	−2.9888 (0)	−2.6124 (0)
10	−4.3077 (0)	−4.5885 (0)	−4.0501 (0)	−3.5099 (0)	−3.1071 (0)
11	−4.5193 (0)	−5.0506 (0)	−4.5980 (0)	−4.0491 (0)	−3.6235 (0)
12	−4.6623 (0)	−5.4914 (0)	−5.1597 (0)	−4.6071 (0)	−4.1626 (0)
13	−4.7340 (0)	−5.9099 (0)	−5.7288 (0)	−5.1846 (0)	−4.7253 (0)

			$b_n(E_0, Al)$ $Z=13$		
n \ E_0(Mev)	0.5	0.7	1.0	1.5	2.0
0	1.0001 (0)	9.9999 (−1)	9.9819 (−1)	9.9641 (−1)	9.9640 (−1)
1	−1.3070 (−1)	−2.5215 (−1)	9.0059 (−2)	2.1928 (−1)	2.7129 (−1)
2	−7.8756 (−1)	−1.2030 (0)	−5.6633 (−1)	−4.0565 (−1)	−3.6339 (−1)
3	−9.8747 (−1)	−1.8585 (0)	−9.6259 (−1)	−8.6972 (−1)	−9.0190 (−1)
4	−7.4740 (−1)	−2.2242 (0)	−1.0904 (0)	−1.1643 (0)	−1.3385 (0)
5	−8.4323 (−2)	−2.3060 (0)	−9.4128 (−1)	−1.2806 (0)	−1.6674 (0)
6	1.1545 (0)	−2.1097 (0)	−5.0695 (−1)	−1.2101 (0)	−1.8828 (0)
7	2.4430 (0)	−1.6409 (0)	2.2099 (−1)	−9.4414 (−1)	−1.9791 (0)
8	4.2732 (0)	−9.0553 (−1)	1.2509 (0)	−4.7400 (−1)	−1.9505 (0)
9	6.4586 (0)	9.0729 (−2)	2.5912 (0)	2.0895 (−1)	−1.7912 (0)
10	8.9821 (0)	1.3421 (0)	4.2502 (0)	1.1134 (0)	−1.4954 (0)
11	1.1827 (1)	2.8321 (0)	6.2364 (0)	2.2479 (0)	−1.0575 (0)
12	1.4976 (1)	4.5870 (0)	8.5580 (0)	3.6213 (0)	−4.7163 (−1)
13	1.8412 (1)	6.5691 (0)	1.1224 (1)	5.2421 (0)	2.6792 (−1)

n \ E_0(Mev)	2.5	3.5	5.5	7.5	9.5
0	9.9700 (−1)	9.9849 (−1)	1.0008 (0)	1.0022 (0)	1.0032 (0)
1	3.2250 (−1)	4.2042 (−1)	5.6586 (−1)	6.5832 (−1)	7.2035 (−1)
2	−2.9618 (−1)	−1.3354 (−1)	1.3872 (−1)	3.7355 (−1)	4.4436 (−1)
3	−8.5539 (−1)	−6.6191 (−1)	−2.8031 (−1)	−1.1564 (−2)	1.7550 (−1)
4	−1.3515 (0)	−1.1632 (0)	−6.9091 (−1)	−3.3714 (−1)	−8.5906 (−2)
5	−1.7808 (0)	−1.6359 (0)	−1.0928 (0)	−6.5622 (−1)	−3.3960 (−1)
6	−2.1397 (0)	−2.0785 (0)	−1.4856 (0)	−9.6859 (−1)	−5.8528 (−1)
7	−2.4251 (0)	−2.4896 (0)	−1.8690 (0)	−1.2741 (0)	−8.2266 (−1)
8	−2.6316 (0)	−2.8676 (0)	−1.2427 (0)	−1.5724 (0)	−1.0515 (0)
9	−2.7573 (0)	−3.2110 (0)	−2.6069 (0)	−1.8635 (0)	−1.2714 (0)
10	−2.7981 (0)	−3.5183 (0)	−2.9598 (0)	−2.1471 (0)	−1.4821 (0)
11	−2.7501 (0)	−3.7882 (0)	−3.3026 (0)	−2.4230 (0)	−1.6834 (0)
12	−2.6098 (0)	−4.0189 (0)	−3.6343 (0)	−2.6910 (0)	−1.8749 (0)
13	−2.3736 (0)	−4.2092 (0)	−3.9548 (0)	−2.9510 (0)	−2.0563 (0)

* See footnote at end of table.

TABLE 3. *Coefficients $b_n(E_0, Z)$ of the power-series buildup factor formulation (18) derived from the Capo [9] β_i polynomial coefficients according to transformation (d), table 2.—Continued

$b_n(E_0, Fe)$ $Z = 26$

n	0.5	0.7	1.0	1.5	2.0
0	1.0025 (0)	9.3280 (−1)	1.0002 (0)	1.0162 (0)	1.0100 (0)
1	1.4156 (−1)	9.3980 (−3)	2.1196 (−1)	3.0483 (−1)	3.6092 (−1)
2	−5.2529 (−1)	−6.6107 (−1)	−4.1423 (−1)	−3.0932 (−1)	−2.1516 (−1)
3	−9.9713 (−1)	−1.0661 (0)	−8.7359 (−1)	−8.2351 (−1)	−7.1552 (−1)
4	−1.2730 (0)	−1.1932 (0)	−1.1632 (0)	−1.2350 (0)	−1.1374 (0)
5	−1.3520 (0)	−1.0298 (0)	−1.2726 (0)	−1.5412 (0)	−1.4781 (0)
6	−1.2332 (0)	−5.6333 (−1)	−1.2028 (0)	−1.7393 (0)	−1.7348 (0)
7	−9.1560 (−1)	2.1860 (−1)	−9.4685 (−1)	−1.8266 (0)	−1.9048 (0)
8	−3.9830 (−1)	1.3286 (0)	−5.0014 (−1)	−1.8004 (0)	−1.9854 (0)
9	3.1965 (−1)	2.7791 (0)	1.4217 (−1)	−1.6581 (0)	−1.9738 (0)
10	1.2392 (0)	4.5827 (0)	9.8487 (−1)	−1.3968 (0)	−1.8672 (0)
11	2.3612 (0)	6.7518 (0)	2.0328 (0)	−1.0139 (0)	−1.6629 (0)
12	3.6868 (0)	9.2991 (0)	3.2907 (0)	−5.0678 (−1)	−1.3582 (0)
13	5.2167 (0)	1.2237 (1)	4.7633 (0)	1.2739 (−1)	−9.5027 (−1)

n	2.5	3.5	5.5	7.5	9.5
0	1.0043 (0)	9.9882 (−1)	9.9768 (−1)	9.9931 (−1)	1.0011 (0)
1	4.1631 (−1)	5.1544 (−1)	6.5356 (−1)	7.3825 (−1)	7.9417 (−1)
2	−1.1129 (−1)	7.8643 (−2)	3.4281 (−1)	5.0375 (−1)	6.0957 (−1)
3	−5.7593 (−1)	−3.0975 (−1)	6.5479 (−2)	2.9451 (−1)	4.4503 (−1)
4	−9.7500 (−1)	−6.4792 (−1)	−1.7841 (−1)	1.0922 (−1)	2.9831 (−1)
5	−1.3059 (0)	−9.3405 (−1)	−3.8883 (−1)	−5.3419 (−2)	1.6714 (−1)
6	−1.5660 (0)	−1.1663 (0)	−5.6575 (−1)	−1.9471 (−1)	4.9286 (−2)
7	−1.7526 (0)	−1.3429 (0)	−7.0913 (−1)	−3.1596 (−1)	−5.7516 (−2)
8	−1.8633 (0)	−1.4620 (0)	−8.1896 (−1)	−4.1847 (−1)	−1.5552 (−1)
9	−1.8953 (0)	−1.5218 (0)	−8.9519 (−1)	−5.0353 (−1)	−2.4696 (−1)
10	−1.8461 (0)	−1.5205 (0)	−9.3780 (−1)	−5.7246 (−1)	−3.3411 (−1)
11	−1.7131 (0)	−1.4562 (0)	−9.4676 (−1)	−6.2656 (−1)	−4.1921 (−1)
12	−1.4935 (0)	−1.3272 (0)	−9.2203 (−1)	−6.6712 (−1)	−5.0452 (−1)
13	−1.1850 (0)	−1.1316 (0)	−8.6360 (−1)	−6.9545 (−1)	−5.9228 (−1)

$b_n(E_0, Sn)$ $Z = 50$

n	0.5	0.7	1.0	1.5	2.0
0	1.0021 (0)	1.0023 (0)	1.0014 (0)	1.0008 (0)	1.0007 (0)
1	4.4293 (−1)	4.7107 (−1)	3.8940 (−1)	3.9964 (−1)	4.5973 (−1)
2	−1.3701 (−1)	−3.7218 (−2)	−1.8271 (−1)	−1.5486 (−1)	−3.2606 (−2)
3	−7.4062 (−1)	−5.2449 (−1)	−7.1325 (−1)	−6.5999 (0)	−4.7447 (−1)
4	−1.3707 (0)	−9.9267 (−1)	−1.2005 (0)	−1.1130 (0)	−8.6409 (−1)
5	−2.0301 (0)	−1.4437 (0)	−1.6428 (0)	−1.5113 (0)	−1.1997 (0)
6	−2.7218 (0)	−1.8796 (0)	−2.0384 (0)	−1.8520 (0)	−1.4794 (0)
7	−3.4484 (0)	−2.3022 (0)	−2.3856 (0)	−2.1326 (0)	−1.7015 (0)
8	−4.2129 (0)	−2.7134 (0)	−2.6827 (0)	−2.3503 (0)	−1.8642 (0)
9	−5.0181 (0)	−3.1153 (0)	−2.9280 (0)	−2.5023 (0)	−1.9657 (0)
10	−5.8668 (0)	−3.5097 (0)	−3.1199 (0)	−2.5861 (0)	−2.0042 (0)
11	−6.7620 (0)	−3.8986 (0)	−3.2566 (0)	−2.5988 (0)	−1.9779 (0)
12	−7.7063 (0)	−4.2839 (0)	−3.3363 (0)	−2.5378 (0)	−1.8850 (0)
13	−8.7028 (0)	−4.6676 (0)	−3.3576 (0)	−2.4004 (0)	−1.7237 (0)

n	2.5	3.5	5.5	7.5	9.5
0	1.0008 (0)	1.0010 (0)	9.9781 (−1)	9.9514 (−1)	9.9484 (−1)
1	5.1974 (−1)	6.1402 (−1)	7.1884 (−1)	7.8769 (−1)	8.3584 (−1)
2	8.8252 (−2)	2.7747 (−1)	4.7050 (−1)	5.9132 (−1)	6.7805 (−1)
3	−2.9304 (−1)	−1.0061 (−2)	2.4198 (−1)	3.8887 (−1)	5.0414 (−1)
4	−6.2353 (−1)	−2.4997 (−1)	1.8862 (−2)	1.6318 (−1)	2.9679 (−1)
5	−9.0259 (−1)	−4.4365 (−1)	−1.9888 (−1)	−1.0291 (−1)	3.8674 (−2)
6	−1.1296 (0)	−5.9248 (−1)	−4.3285 (−1)	−4.2656 (−1)	−2.8753 (−1)
7	−1.3039 (0)	−6.9785 (−1)	−6.9027 (−1)	−8.2495 (−1)	−6.9916 (−1)
8	−1.4250 (0)	−7.6116 (−1)	−9.8197 (−1)	−1.3152 (0)	−1.2135 (0)
9	−1.4921 (0)	−7.8379 (−1)	−1.3188 (0)	−1.9146 (0)	−1.8480 (0)
10	−1.5048 (0)	−7.6713 (−1)	−1.7204 (0)	−2.6401 (0)	−2.6198 (0)
11	−1.4622 (0)	−7.1256 (−1)	−2.1708 (0)	−3.5090 (0)	−3.5463 (0)
12	−1.3639 (0)	−6.2149 (−1)	−2.7078 (0)	−4.5385 (0)	−4.6449 (0)
13	−1.2093 (0)	−4.9529 (−1)	−3.3331 (0)	−5.7457 (0)	−5.9328 (0)

*See footnote at end of table.

TABLE 3. *Coefficients $b_n(E_0, Z)$ of the power-series buildup factor formulation (18) derived from the Capo [9] β_i polynomial coefficients according to transformation (d), table 2.—Continued

$b_n(E_0, \text{W}) \quad Z=74$

n / E_0(Mev)	0.5	0.7	1.0	1.5	2.0
0	1.0086 (0)	1.0089 (0)	1.0032 (0)	9.9925 (−1)	9.9840 (−1)
1	7.3645 (−1)	7.1129 (−1)	5.6840 (−1)	5.2793 (−1)	5.6382 (−1)
2	4.3004 (−1)	3.9926 (−1)	−1.1129 (−1)	3.9821 (−2)	1.2485 (−1)
3	8.5826 (−2)	6.7224 (−2)	−3.7041 (−1)	−4.6593 (−1)	−3.2002 (−1)
4	−2.9946 (−1)	−2.9038 (−1)	−8.7895 (−1)	−9.9020 (−1)	−7.7231 (−1)
5	−7.2925 (−1)	−6.7911 (−1)	−1.4166 (0)	−1.5338 (0)	−1.2335 (0)
6	−1.2069 (0)	−1.1880 (0)	−1.9855 (0)	−2.0977 (0)	−1.7052 (0)
7	−1.7358 (0)	−1.5723 (0)	−2.5880 (0)	−2.6827 (0)	−2.1888 (0)
8	−2.3194 (0)	−2.0878 (0)	−3.2264 (0)	−3.2897 (0)	−2.6859 (0)
9	−2.9610 (0)	−2.6567 (0)	−3.9028 (0)	−3.9195 (0)	−3.1979 (0)
10	−3.6640 (0)	−3.2846 (0)	−4.6195 (0)	−4.5729 (0)	−3.7265 (0)
11	−4.4317 (0)	−3.9770 (0)	−5.3788 (0)	−5.2510 (0)	−4.2740 (0)
12	−5.2677 (0)	−4.7396 (0)	−6.1829 (0)	−5.9545 (0)	−4.8390 (0)
13	−6.1752 (0)	−5.5767 (0)	−7.0341 (0)	−6.6842 (0)	−5.4261 (0)

n / E_0(Mev)	2.5	3.5	5.5	7.5	9.5
0	9.9844 (−1)	9.9910 (−1)	9.9375 (−1)	9.8630 (−1)	9.8003 (−1)
1	6.1013 (−1)	6.8979 (−1)	7.6125 (−1)	7.8912 (−1)	7.9744 (−1)
2	2.2914 (−1)	4.0578 (−1)	5.3024 (−1)	5.6254 (−1)	5.6596 (−1)
3	−1.4706 (−1)	1.4271 (−1)	2.8324 (−1)	2.8009 (−1)	2.5718 (−1)
4	−5.2100 (−1)	−1.0380 (−1)	2.7784 (−3)	−8.4723 (−2)	−1.5728 (−1)
5	−8.9521 (−1)	−3.3811 (−1)	−3.2861 (−1)	−5.5836 (−1)	−7.0582 (−1)
6	−1.2722 (0)	−5.6459 (−1)	−7.2839 (−1)	−1.1673 (0)	−1.4168 (0)
7	−1.6545 (0)	−7.8762 (−1)	−1.2140 (0)	−1.9381 (0)	−2.3187 (0)
8	−2.0446 (0)	−1.0116 (0)	−1.8030 (0)	−2.8971 (0)	−3.4398 (0)
9	−2.4452 (0)	−1.2408 (0)	−2.5128 (0)	−4.0708 (0)	−4.8086 (0)
10	−2.8585 (0)	−1.4797 (0)	−3.3608 (0)	−5.4858 (0)	−6.4533 (0)
11	−3.2873 (0)	−1.7326 (0)	−4.3646 (0)	−7.1685 (0)	−8.4026 (0)
12	−3.7341 (0)	−2.0039 (0)	−5.5416 (0)	−9.1453 (0)	−1.0685 (1)
13	−4.2013 (0)	−2.2979 (0)	−6.9093 (0)	−1.1443 (1)	−1.3328 (1)

$b_n(E_0, \text{Pb}) \quad Z=82$

n / E_0(Mev)	0.5	0.7	1.0	1.5	2.0
0	9.9993 (−1)	1.0087 (0)	1.0159 (0)	1.0171 (0)	1.0109 (0)
1	7.5580 (−1)	7.1782 (−1)	6.7548 (−1)	6.3718 (−1)	6.2940 (−1)
2	4.7600 (−1)	3.9601 (−1)	3.1164 (−1)	2.4664 (−1)	2.4906 (−1)
3	1.5697 (−1)	4.0094 (−2)	−7.5640 (−2)	−1.5563 (−1)	−1.3025 (−1)
4	−2.0485 (−1)	−3.5310 (−1)	−4.9597 (−1)	−5.7075 (−1)	−5.0870 (−1)
5	−6.1301 (−1)	−7.8673 (−1)	−9.4455 (−1)	−9.9981 (−1)	−8.8649 (−1)
6	−1.0711 (0)	−1.2639 (0)	−1.4262 (0)	−1.4439 (0)	−1.2638 (0)
7	−1.5826 (0)	−1.7879 (0)	−1.9433 (0)	−1.9042 (0)	−1.6407 (0)
8	−2.1512 (0)	−2.3618 (0)	−2.4982 (0)	−2.3818 (0)	−2.0175 (0)
9	−2.7804 (0)	−2.9887 (0)	−3.0934 (0)	−2.8777 (0)	−2.3944 (0)
10	−3.4737 (0)	−3.6718 (0)	−3.7314 (0)	−3.3931 (0)	−2.7714 (0)
11	−4.2347 (0)	−4.4144 (0)	−4.4144 (0)	−3.9291 (0)	−3.1488 (0)
12	−5.0669 (0)	−5.2194 (0)	−5.1449 (0)	−4.4869 (0)	−3.5267 (0)
13	−5.9709 (0)	−6.0901 (0)	−5.9253 (0)	−5.0674 (0)	−3.9054 (0)

n / E_0(Mev)	2.5	3.5	5.5	7.5	9.5
0	1.0026 (0)	9.9132 (−1)	1.0012 (0)	9.9279 (−1)	9.6581 (−1)
1	6.4235 (−1)	6.9948 (−1)	8.0216 (−1)	8.0445 (−1)	8.0326 (−1)
2	2.9304 (−1)	4.2933 (−1)	6.1069 (−1)	5.8826 (−1)	5.9791 (−1)
3	−4.5410 (−2)	1.7884 (−1)	4.1282 (−1)	3.2014 (−1)	3.2578 (−1)
4	−3.7250 (−1)	−5.4018 (−2)	1.9459 (−1)	−2.4004 (−2)	−3.7126 (−2)
5	−6.8858 (−1)	−2.7128 (−1)	−5.7996 (−2)	−4.6826 (−1)	−5.1480 (−1)
6	−9.9345 (−1)	−4.5468 (−1)	−3.5890 (−1)	−1.0367 (0)	−1.1312 (0)
7	−1.2870 (0)	−6.6715 (−1)	−7.2210 (−1)	−1.7535 (0)	−1.9104 (0)
8	−1.5693 (0)	−8.4981 (−1)	−1.1616 (0)	−2.6426 (0)	−2.8763 (0)
9	−1.8401 (0)	−1.0250 (0)	−1.6913 (0)	−3.7282 (0)	−4.0529 (0)
10	−2.0994 (0)	−1.1947 (0)	−2.3252 (0)	−5.0344 (0)	−5.4642 (0)
11	−2.3472 (0)	−1.3611 (0)	−3.0774 (0)	−6.5852 (0)	−7.1342 (0)
12	−2.5833 (0)	−1.5260 (0)	−3.9617 (0)	−8.4047 (0)	−9.0869 (0)
13	−2.8077 (0)	−1.6916 (0)	−4.9921 (0)	−1.0517 (1)	−1.1346 (1)

*See footnote at end of table.

TABLE 3. *Coefficients $b_n(E_0, Z)$ of the power-series buildup factor formulation (18) derived from the Capo [9] β_i polynomial coefficients according to transformation (d), table 2.—Continued

n	E_0(Mev) 0.5	0.7	1.0	1.5	2.0
0	1.0107 (0)	1.0087 (0)	1.0061 (0)	1.0033 (0)	1.0017 (0)
1	8.3176 (−1)	7.8986 (−1)	7.4124 (−1)	6.9250 (−1)	6.7550 (−1)
2	6.2417 (−1)	5.4367 (−1)	4.5187 (−1)	3.6412 (−1)	3.3996 (−1)
3	3.8503 (−1)	2.6744 (−1)	1.3578 (−1)	1.6510 (−2)	−6.1238 (−3)
4	1.1141 (−1)	−4.1481 (−2)	−2.0928 (−1)	−3.5196 (−1)	−3.6398 (−1)
5	−1.9961 (−1)	−3.8575 (−1)	−5.8553 (−1)	−7.4292 (−1)	−8.4503 (−1)
6	−5.5096 (−1)	−7.6800 (−1)	−9.9522 (−1)	−1.1580 (0)	−1.1199 (0)
7	−9.4557 (−1)	−1.1909 (0)	−1.4406 (0)	−1.5989 (0)	−1.5204 (0)
8	−1.3864 (0)	−1.6571 (0)	−1.9239 (0)	−2.0671 (0)	−1.9376 (0)
9	−1.8763 (0)	−2.1692 (0)	−2.4473 (0)	−2.5644 (0)	−2.3726 (0)
10	−2.4182 (0)	−2.7299 (0)	−3.0131 (0)	−3.0923 (0)	−2.8268 (0)
11	−3.0151 (0)	−3.3419 (0)	−3.6236 (0)	−3.6526 (0)	−3.3013 (0)
12	−3.6699 (0)	−4.0078 (0)	4.2809 (0)	−4.2467 (0)	−3.7974 (0)
13	−4.3854 (0)	−4.7301 (0)	−4.9874 (0)	−4.8764 (0)	−4.3163 (0)

n	E_0(Mev) 2.5	3.5	5.5	7.5	9.5
0	1.0010 (0)	1.0006 (0)	9.9775 (−1)	9.8835 (−1)	9.8163 (−1)
1	6.8131 (−1)	7.3122 (−1)	8.3551 (−1)	8.2590 (−1)	8.0789 (−1)
2	3.6080 (−1)	4.7491 (−1)	6.8739 (−1)	6.4374 (−1)	5.9135 (−1)
3	3.8355 (−2)	2.2977 (−1)	5.4509 (−1)	4.2402 (−1)	3.1040 (−1)
4	−2.8712 (−1)	−6.1556 (−3)	4.0033 (−1)	1.4889 (−1)	−5.6604 (−2)
5	−6.1672 (−1)	−2.3480 (−1)	2.4481 (−1)	−1.9951 (−1)	−5.3128 (−1)
6	−9.5156 (−1)	−4.5812 (−1)	7.0266 (−2)	−6.3902 (−1)	−1.1353 (0)
7	−1.2927 (0)	−6.7804 (−1)	−1.3165 (−1)	−1.1875 (0)	−1.8902 (0)
8	−1.6413 (0)	−8.9653 (−1)	−3.6916 (−1)	−1.8628 (0)	−2.8176 (0)
9	−1.9985 (0)	−1.1153 (0)	−6.5058 (−1)	−2.6828 (0)	−3.9393 (0)
10	−2.3653 (0)	−1.3369 (0)	−9.8419 (−1)	−3.6653 (0)	−5.2767 (0)
11	−2.7428 (0)	−1.5628 (0)	−1.3783 (0)	−4.8282 (0)	−6.8516 (0)
12	−3.1321 (0)	−1.7949 (0)	−1.8412 (0)	−6.1893 (0)	−8.6856 (0)
13	−3.5344 (0)	−2.0353 (0)	−2.3811 (0)	−7.7665 (0)	−1.0800 (1)

* The figures in parentheses in tables 3, 4, and 5 indicate the power of 10 by which the adjacent entry is to be multiplied; e.g., $6.4656\ (-2) = 0.064656$.

6. Utility and Limitations of the Power-Series Method

With respect to use of the infinite series (19), gamma-ray distributed source problems fall into three classes:

(a) In the region $0 \leq \mu_0 x \lesssim 0.01$, as is often the case in an air medium [29], all terms in (19) may be neglected except for the zeroth term $(\sigma/4\pi)\,q_0$ (geom). This term is the complete solution for pure inverse square law attenuation as assumed by Meredith [29], and depends only on relative rather than absolute dimensions of the detector-source geometry.

(b) In the region $0.01 \lesssim \mu_0 x \lesssim 1.0$ the series (19) has its greatest usefulness, either with or without inclusion of scattered radiation by $b_n(E_0, Z)$ coefficients. This will be demonstrated in the numerical examples in section 7.

(c) In the region $1.0 \lesssim \mu_0 x < \infty$, as is the case in fallout shelter calculations, the series (19) is usually *not* useful, and recourse must be made to other available methods [1, 2].

It is interesting to note that the speed of convergence of (19) is usually *enhanced* over that for (15), rather than the converse. A possible explanation for this enhancement (with no attempt at a proof) is offered as follows:

In an absorbing and scattering medium the point-source buildup factor $B_{\text{PTI}}(E_0, Z, r)$ is bounded, roughly, by the limits

$$1 \leq B_{\text{PTI}}(E_0, Z, r) \lesssim \exp(+\mu_0 r). \qquad (20)$$

The lower bound, $B_{\text{PTI}}(E_0, Z, r) = 1$, corresponding to *pure absorption* $(D^s = 0$ in eq (1)), would lead to buildup coefficients all equal to unity, i.e.,

$$b_n(E_0, Z) = 1, \qquad n = 0, 1, 2, \ldots \qquad (21)$$

in which case (19) would be identical with (15). The upper *approximate* bound, $B_{\text{PTI}}(E_0, Z, r) = \exp(+\mu_0 r)$, corresponding to a *pure scatterer* (photons may be scattered, but never absorbed or degraded in energy) is the same as simple inverse-square-law attenuation, such that the point-source eq (2) would reduce to

$$D = (k/4\pi)/r^2. \qquad (22)$$

This buildup-factor behavior can be applied to (19) by setting all except the zeroth buildup coefficient equal to zero, i.e.,

$$b_0(E_0, Z) = 1$$

$$b_{n \geq 1}(E_0, Z) = 0, \qquad n = 1, 2, 3, \ldots \quad (23)$$

Hence, in the intermediate region indicated in (20) we might expect the observed enhancement.

7. Numerical Examples

7.1. Example 1. Rectangular Co–60 Source, Stratified Barrier of Steel and Water. Comparison With Experiment

There exist little experimental data in the moderate-penetration region $0.01 \lesssim \mu_0 x \lesssim 1.0$, discussed in (b) of the preceding section, for simple geometries amenable to direct analysis using (19). However, in connection with food irradiator design studies [17] data have been published for the more complicated situation of a two-layer barrier. Here, Donovan [30] measured the dose-rate received by a detector separated from a rectangular Co–60 source by a 3-in. layer of water and varying thicknesses of steel cladding as shown in figure 3. These results are over the range $0.589 \leq \mu_0 x (\text{water} + \text{steel}) \leq 1.225$, hence they provide an excellent check on (19) up to the upper limit of its usefulness as discussed in (b) of the preceding section.

The agreement between theory (infinite homogeneous medium) and experiment (layered inhomogeneous medium) in the following example must be considered somewhat fortuitous, although the position of the detector *within* the water phantom tends to minimize boundary effects. Since interest has been expressed in adapting eq (19) for use in nuclear engineering curricula, this example is presented in great detail, particularly in the steps involving dimensional analysis.

a. Situation

A 6-in. thick water-equivalent slab phantom is separated by an airgap of 2.5 in. from a 50-in. wide by 57-in. long rectangular plaque Co–60 source. This source, with a uniform activity of 1 curie per cm² of area, is encased in steel cladding of uniform thickness.

b. Problem

Find the dose-rate (rads [31] in H_2O) in the center of the phantom as the thickness of steel cladding is varied from 0.097 in. to 0.679 in. Use the simplifying approximations:

(1) To take into account the finite thickness of the source (Co, $Z = 27$), include half the source thickness in the thickness of steel (Fe, $Z = 26$) representing "cladding thickness" in the calculation, as was done in an alternative analytical study of this problem [3].

(2) Assume that the Co–60 nuclides emit two 1.25-Mev photons per disintegration, rather than a 1.17 Mev and a 1.33 Mev photon as is actually the case.
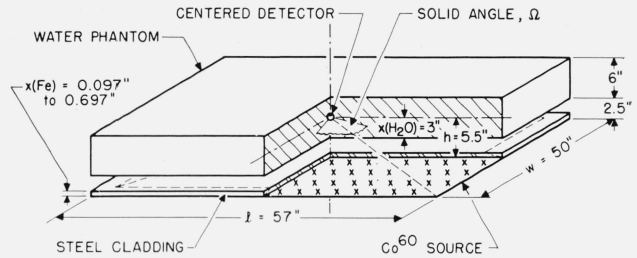

FIGURE 3. *Donovan [30] food irradiator rectangular source geometry treated in example 1.*

(3) Kalos ([21], page 796) has shown that for a composite barrier consisting of a layer of high-Z material followed by a layer of low-Z material, the resulting buildup factor shows a smooth rise from the value for pure high-Z material toward that for pure low-Z material, the rate of approach depending on the source energy. Indeed, substitution of the linear approximation (6) for $B_{\text{PTI}}(E_0, Z, r)$ in Kalos' empirical eq [21], (26.4) gives the linear connecting form

$$B_{\text{PTI}}(E_0, Z_1, Z_2, r_1 + r_2)$$

$$= \frac{\mu_0(Z_1) r_1}{\mu_0(Z_1) r_1 + \mu_0(Z_2) r_2} B_{\text{PTI}}(E_0, Z_1, r_1)$$

$$+ \frac{\mu_0(Z_2) r_2}{\mu_0(Z_1) r_1 + \mu_0(Z_2) r_2} B_{\text{PTI}}(E_0, Z_2, r_2) \quad (24)$$

in which Z_1, r_1 refer to one layer of the barrier and Z_2, r_2 refer to the other layer of the barrier. Since the buildup for iron and for water are not greatly different [32] over the penetration range in this problem, the approximate combinatorial form (24) will be used.

c. Plan of Attack

Evaluate the dose rate (rads in H_2O/hr) using (19) assuming the medium (a) to be all water:

$$D(H_2O) = (\sigma/4\pi) \sum_{n=0}^{\infty} b_n(1.25 \text{ Mev}, H_2O) \cdot q_n(\text{geom}) \cdot (\mu_0 x)^n$$
$$(19a)$$

and (b) to be all steel:

$$D(\text{Fe}) = (\sigma/4\pi) \sum_{n=0}^{\infty} b_n(1.25 \text{ Mev}, \text{Fe}) \cdot q_n(\text{geom}) \cdot (\mu_0 x)^n$$
$$(19b)$$

in which (19a) and (19b) differ only in the values of the buildup factor coefficients $b_n(E_0, Z)$. Then use (24) to obtain a dose rate between these upper and lower bounds by weighting the results from (19a) and (19b) by the fractions of mean-free-path distance traversed by the primary photons in each material:

$$D = \{(\mu_0 x)_{H_2O}/(\mu_0 x)_{\text{total}}\} D(H_2O)$$

$$+ \{(\mu_0 x)_{\text{Fe}}/(\mu_0 x)_{\text{total}}\} D(\text{Fe}). \quad (25)$$

d. Source Strength Constant $(\sigma/4\pi)$

For an answer from (19) in units of rads/hr per curie/cm² of source strength, the factor $(\sigma/4\pi)$ is

$$(\sigma/4\pi) = 1.7005 \times 10^5 \times N(\text{photons of energy } E_0/\text{disintegration}) \times E_0 \text{ (Mev/photon)} \times \{\mu_{en}(E_0, Z)/\rho\} \text{ (cm}^2/\text{g)} \quad (26)$$

in which the numerical constant 1.7005×10^5 is obtained from the dimensional factors

$$1.7005 \times 10^5 = (1/4\pi) \text{ (steradians}^{-1}) \times 3.71 \times 10^{10}$$

$$\{(\text{disintegrations/sec})/\text{curie}\} \times 1.6 \times 10^{-8} \{\text{rads}/$$

$$(\text{Mev/g})\} \times 3.6 \times 10^3 \text{ (sec/hr)} \quad (27)$$

For the problem stated above the numerical values of the other constants in (26) are

$$N = 2 \text{ photons/disintegration}$$

$$E_0 = 1.25 \text{ Mev/photon, and}$$

$$\mu_{en}(1.25 \text{ Mev, H}_2\text{O})/\rho = 0.0296 \text{ cm}^2/\text{g.}^5$$

Substitution of these values in (26) gives a source strength constant $(\sigma/4\pi)$ of

$$(\sigma/4\pi) = 1.258 \times 10^4$$

for values of $D(\text{H}_2\text{O})$ and $D(\text{Fe})$ from (19a) and (19b) in units of $\{\text{rads (H}_2\text{O})/\text{hr}\}/\{\text{curies/cm}^2\}$.

e. Buildup Factor Coefficients $b_n (E_0, Z)$

Since reference [9] and hence table 3 of this work do not contain data at 1.25 Mev, some interpolation is required to obtain the $b_n(E_0, Z)$ series coefficients needed in (19a) and (19b). This interpolation is conveniently performed on the "untransformed" $\beta_i(E_0, Z)$ *polynomial* coefficients, from which any number of $b_n(E_0, Z)$ *series* coefficients may be generated using (d), table 2. Table 4 contains polynomial coefficients:

(a) $\beta_i(1.25 \text{ Mev, H}_2\text{O})$ interpolated from [25],[6] table 2, and

(b) $\beta_i(1.25 \text{ Mev, Fe})$ interpolated from [9], table 7B

---

[5] Interpolated from [24], table 2.
[6] The coefficients in [25] as in [9] were fitted to the calculated results in NYO–3075[26].

TABLE 4. *Polynomial buildup factor coefficients $\beta_i(E_0, Z)$ used as input data in examples 1 and 2*

i	$\beta_i(1.25 \text{ Mev, H}_2\text{O})$*	$\beta_i(1.25 \text{ Mev, Fe})$**
0	1.00 (0)	1.013 (0)
1	9.00 (−1)	7.455 (−1)
2	1.40 (−1)	6.055 (−2)
3	−3.90 (−3)	−5.320 (−4)

*Interpolated from reference [25], table 2.
**Interpolated from reference [9], table 7B.

Corresponding values of $b_n(1.25 \text{ Mev, H}_2\text{O})$ and $b_n(1.25 \text{ Mev, Fe})$, computed using the numbers in table 4 as input values for formula (d), table 2, are given in table 5 for $0 \le n \le 30$ and are ready for use in (19a) and (19b).

TABLE 5. *Buildup factor and geometry data used in example 1, series solutions (19a) and (19b).*

The $b_n(E_0, Z)$ coefficients, of which $b_n(1.25 \text{ Mev, H}_2\text{O})$ were also used in example 2, eq (19c), were derived from table 4 using transformation (d), table 2. The $q_n(\text{geom})$ geometry coefficients were obtained from [7], table 3 (and unpublished higher coefficients from formulas (57) and (58), as

$$q_n(\text{Donovan geom}) = 4q_n(a, b)$$

using $a = (w/2)/h = 5$, $b = (l/2)/h = 5$ and the factor of four to apply the detector-over-corner data to Donovan's centered-detector geometry. For $h = 5.5$ in., these a and b values imply plaque dimensions of 55 by 55 in., rather than Donovan's 50 by 57 in. However, the solid angles subtended in each case differ by less than 1 percent.

n	$b_n(1.25 \text{ Mev, H}_2\text{O})$	$b_n(1.25 \text{ Mev, Fe})$	$q_n(\text{geom})$
0	1.000 (0)	1.013 (0)	1.090 (1)
1	1.000 (−1)	2.670 (−1)	−2.953 (1)
2	−5.200 (−1)	−3.574 (−1)	5.000 (2)
3	−8.366 (−1)	−8.575 (−1)	−6.638 (1)
4	−8.264 (−1)	−1.230 (0)	7.361 (1)
5	−4.660 (−1)	−1.472 (0)	−7.022 (1)
6	2.680 (−1)	−1.580 (0)	5.878 (1)
7	1.399 (0)	−1.551 (0)	−4.388 (1)
8	2.950 (0)	−1.382 (0)	2.959 (1)
9	4.946 (0)	−1.069 (0)	−1.822 (1)
10	7.408 (0)	−6.100 (−1)	1.032 (1)
11	1.036 (1)	−8.200 (−4)	−5.424 (0)
12	1.383 (1)	7.613 (−1)	2.658 (0)
13	1.783 (1)	1.680 (0)	−1.220 (0)
14	2.240 (1)	2.757 (0)	5.274 (−1)
15	2.755 (1)	3.998 (0)	−2.152 (−1)
16	3.330 (1)	5.404 (0)	8.322 (−2)
17	3.969 (1)	6.979 (0)	−3.057 (−2)
18	4.673 (1)	8.726 (0)	1.069 (−2)
19	5.445 (1)	1.065 (1)	−3.570 (−3)
20	6.288 (1)	1.275 (1)	1.140 (−3)
21	7.167 (1)	1.499 (1)	−3.488 (−4)
22	8.192 (1)	1.750 (1)	1.024 (−4)
23	9.258 (1)	2.016 (1)	−2.890 (−5)
24	1.040 (2)	2.300 (1)	7.852 (−6)
25	1.163 (2)	2.605 (1)	−2.056 (−6)
26	1.294 (2)	2.929 (1)	5.197 (−7)
27	1.434 (2)	3.273 (1)	−1.251 (−7)
28	1.583 (2)	3.577 (1)	2.998 (−8)
29	1.741 (2)	4.022 (1)	−6.857 (−9)
30	1.908 (2)	4.429 (1)	1.520 (−9)

f. Geometry Coefficients $q_n(\text{geom})$

The parameters describing Donovan's experimental geometry, as shown in figure 3 are:

w = plaque width = **50 in.**

l = plaque length = **57 in.**

h = distance (height) of detector above plaque center

= 2.5 in. airgap + 3 in. water

= **5.5 in.**

In the notation of [7] the geometry coefficients for this centered-detector situation could be calculated exactly as

$$q_n(\text{Donovan geometry}) = 4q_n(a, b) \quad (28)$$

where $q_n(a, b)$ are corner-position rectangular-source geometry coefficients and

$$a = (w/2)/h = (50/2)/5.5 = 4.54\overline{54}$$

$$b = (l/2)/h = (57/2)/5.5 = 5.18\overline{18} \qquad (29)$$

However, $q_n(a, b)$ values for $a = 5$, $b = 5$ are already available in [7] for $0 \leq n \leq 9$ and in unpublished form for $0 \leq n \leq 35$. We can use these tabulated coefficients and avoid a two-way interpolation, or an exact calculation of $q_n(\text{geom})$ coefficients from formulas in [7], by the following argument:

It has been noted [1–3] that geometry effects scale approximately as the solid angle, Ω,[7] subtended by the source from the detector for barrier thicknesses of the order of one mean-free-path. Hence, since the solid angle corresponding to the already tabulated coefficients differs from the solid angle in Donovan's geometry by less than a percent, i.e.,

$$\Omega(a = 5, b = 5)/\Omega(a = 4.54\overline{54}, b = 5.18\overline{18})$$

$$= 4p_0(5, 5)/4p_0(4.54\overline{54}, 5.18\overline{18})$$

$$= 5.170 \text{ steradians}/5.132 \text{ steradians}$$

$$= \mathbf{1.007} \qquad (30)$$

the available coefficients for $a = 5$, $b = 5$ are used according to (19) and are given as the last column of table 5 for $0 \leq n \leq 30$.

g. Penetration Thickness $\mu_0 x$

The last factor, $(\mu_0 x)^n$, in each series term of (19a) and (19b) is for this problem simply the n'th power of the barrier thickness in mean free paths (abbreviated mfp). If this thickness is given in inches, the thickness in mfp is

$$\mu_0 x(\text{mfp}) = \mu(E_0, Z)(\text{cm}^2/\text{g}) \times \rho(\text{g/cm}^3)$$

$$\times 2.54 \text{ (cm/in.)} \times x(\text{in.}) \quad (31)$$

where $\mu(E_0, Z)$ is the narrow-beam attenuation coefficient [23] as used in (2) and ρ is the density of the medium.

For 1.25 Mev gammas in water we see that

$$\mu_0 x(\text{mfp})/x(\text{in.}) = 0.0634 \text{ (cm}^2/\text{g)}$$

$$\times 1.00 \text{ (g/cm}^3) \times 2.54 \text{ (cm/in.)}$$

$$= \mathbf{0.161} \text{ mfp/(in. of water)} \qquad (32)$$

and similarly for iron that

$$\mu_0 x(\text{mfp})/x(\text{in.}) = 0.0533 \text{ (cm}^2/\text{g)}$$

$$\times 7.83 \text{ (g/cm}^3) \times 2.54 \text{ (cm/in.)}$$

$$= \mathbf{1.06} \text{ mfp/(in. of steel)}. \qquad (33)$$

---

[7] This solid angle, Ω, is identical with the tabulated quantity $p_0(\text{geom})$ in [7] {i.e., $p_0(a, b)$} and [8] {i.e., $p_0(\rho, h)$}.

Thus, for example,

$$3 \text{ in. water} = 3 \text{ in.} \times 0.161 \text{ mfp/in.} = 0.483 \text{ mfp},$$

and

$$0.097 \text{ in. steel} = 0.097 \text{ in.} \times 1.06 \text{ mfp/in.} = 0.103 \text{ mfp}.$$

h. Numerical Results, D^0 and D

Donovan's measured values of D for 3 in. of water preceded by various thicknesses of steel [30] are shown in figure 4, with his estimated ± 3 percent uncertainty indicated [33].

Before evaluating the total dose D according to (19a), (19b), and (25), it is of some interest to first evaluate the unscattered component D^0 according to (15). We can then note the effect of buildup as characterized by the $b_n(E_0, Z)$ coefficients. Inserting the data from the preceding sections (d), (f), and (g) in (15), sums for a variety of $\mu_0 x$ values yield D^0 (curve (a) in fig. 4) which is independent of the kind of medium and the photon energy except for the source strength factor $\sigma/4\pi$. Indeed, except for the factor $\sigma/4\pi$ the data for curve (a) are already tabulated in [7], table 4.

Next we can evaluate $D(H_2O)$ and $D(Fe)$ from (19a) and (19b) using the same set of summations as for D^0 (curve (a), above) except that each series term is multiplied by the appropriate buildup factor coefficient $b_n(E_0, Z)$ from table 5. These sums $D(H_2O)$ and $D(Fe)$ (for Donovan's geometry embedded in infinite media of water and steel, respectively) are displayed as curves (b) and (c) in figure 4. The circled numbers are a qualitative indication of the convergence rate of (19) and are, for the indicated calculated points, the number of the series term ($n+1$, including the zeroth term) beyond which the partial sum remains within 0.1 percent of the sum up to $n=30$.

Weighting $D(H_2O)$ and $D(Fe)$ (curves (b) and (c)) according to (25) we obtain D, the hybrid curve (d), our desired result.

The calculated values of D in curve (d) can now be compared *absolutely* with Donovan's measured values, since the method is free of any arbitrary normalization. Agreement is seen to be within Donovan's 3 percent estimated uncertainty.

The results of a more approximate but simpler analysis by Moote [3] are shown as curve (e). In this analysis, which gives an excellent fit to the data in the neighborhood of $\mu_0 x = 1$, the dose rate D is given as the simple product of:

(a) The source strength constant $\sigma/4\pi$,

(b) the solid angle Ω, indicated in figure 3, subtended by the source from the detector,

(c) the exponential integral $E_1(\mu_0 x)$ for the total barrier thickness $\mu_0 x$, and

(d) the *plane* isotropic source buildup factor, $B_{\text{PLI}}(E_0, H_2O, \mu_0 x)$, for the dose rate at a distance $\mu_0 x$ from an infinite plane source in water.
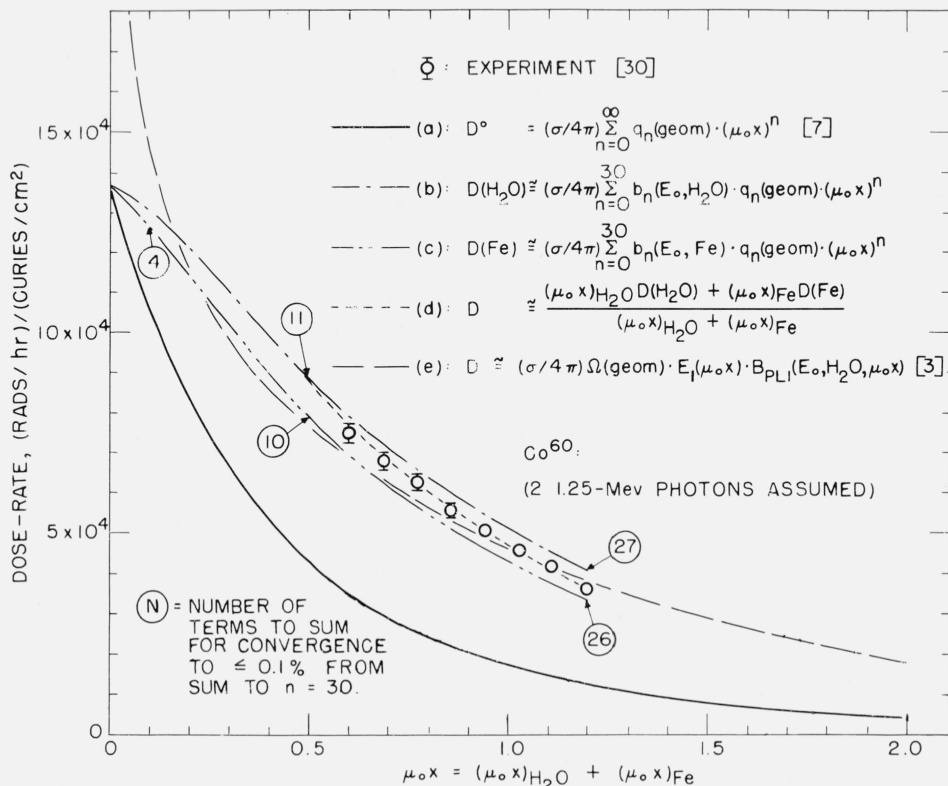
FIGURE 4. *Results for the Donovan food irradiator rectangular source geometry (example 1).*

Donovan's experimental points [30, 33] are compared with the theoretical results:
(a) The dose-rate component D^0 due to primaries (eq 15).
(b) The total dose-rate $D(H_2O)$ assuming an all-water medium (eq 19a).
(c) The total dose-rate $D(Fe)$ assuming an all-iron medium (eq 19b).
(d) A weighted average, D, of curves (b) and (c) according to (25).
(e) The total dose-rate, D, according to the solid-angle exponential-integral approximation used by Moote [3].

7.2. Example 2. Dose-Rate Profiles Across a Cleared Circular Area in a Co–60 Infinite Plane Source in Air

Along the *axis* of a circular disk source, analytic solutions for the flux in terms of exponential integrals and the buildup formulations [9, 11–15] are well known. However, *off-axis* solutions including build-up data have *not*, to the author's knowledge, yet appeared in the literature. The power-series solution (19) *does* apply to this situation, as will be illustrated in this example.

a. Situation

A circular area 600 ft in diameter has been cleared in an infinite plane isotropic source of 1 curie/ft^2 of Co–60. The surrounding medium is air (no ground-air interface is taken into account).

b. Problem

Find dose-rate profiles, relative to the undisturbed infinite plane source, at heights 3 ft (0.00626 mfp), 30 ft (0.0626 mfp) and 300 ft (0.626 mfp) above the plane of the source. Buildup data for air are not available in parametric form [9, 11–15], but water buildup data can be used to good approximation [1, 2].

c. Plan of Attack

Evaluate the dose-rates (rads/hr in air) at $h=3$, 30, and 300 ft above the infinite plane source [25, 34] using $\beta_i(E_0, Z)$ coefficients from the polynomial buildup formula (10) according to

$$D_{\text{PLI}}(h) = (\sigma/4\pi)2\pi[E_1(\mu_0 h)$$
$$+ \exp(-\mu_0 h)\{\beta_1 + \beta_2 + 2\beta_3$$
$$+ (\beta_2 + 2\beta_3)\mu_0 h + \beta_3(\mu_0 h)^2\}] \quad (34)$$

in which $E_1(\mu_0 h)$ is the ordinary exponential integral [35] and values $\beta_i(1.25 \text{ Mev}, H_2O)$ are already given in table 4. Then, using the derived values $b_n(1.25 \text{ Mev}, H_2O)$ from table 5, evaluate dose-rate profiles across a 600-ft diam disk source with the same source strength constant $(\sigma/4\pi)$ according to (19)

$$D_{\text{DISK}}(\rho, h) = (\sigma/4\pi)\sum_{n=0}^{\infty} b_n (1.25 \text{ Mev}, H_2O)$$
$$\cdot q_n(\rho, h) \cdot (\mu_0 h)^n \quad (19c)$$

where $q_n(\rho, h)$ geometry coefficients are available in [8] for $0 \leq \rho \leq 10$ disk radii and $0.1 \leq h \leq 10$ disk radii, and in unpublished form for $0.01 \leq h \leq 0.1$. In this problem, h assumes the values 0.01, 0.1, and 1.0 disk radii while the penetration thickness $\mu_0 h$ assumes the corresponding values 0.00626, 0.0626, and 0.626 mfp given in the problem.

d. Numerical Results

Evaluation of (34) using the source strength constant $\sigma/4\pi = 12.24$ (rads in air/hr)/(curies/ft^2)[8] gives infinite-plane dose-rates $D_{PLI}(h)$ of 423.7, 247.6, and 78.83 (rads in air/hr)/(curies/ft^2) for the heights 3, 30, and 300 ft, respectively, as indicated by the horizontal lines in figure 5. Summation of (19c) for these three heights and a number of ρ-values gives the dose-rate profiles $D_{DISK}(\rho, h)$ also shown in figure 5. The circled numbers, as in example 1, indicate the required number of series terms for convergence to within 0.1 percent of the stable value.

Subtraction of $D_{DISK}(\rho, h)$ from $D_{PLI}(h)$ gives the desired profiles shown in figure 6, normalized to 100 percent for each infinite plane source result $D_{PLI}(h)$, as specified in the problem.

---

[8] This value of $\sigma/4\pi$ is equivalent to the Clarke and Buchanan ([34], table 1) value of 14.0 (roentgens/hr)/(curies/ft^2) for Co–60.
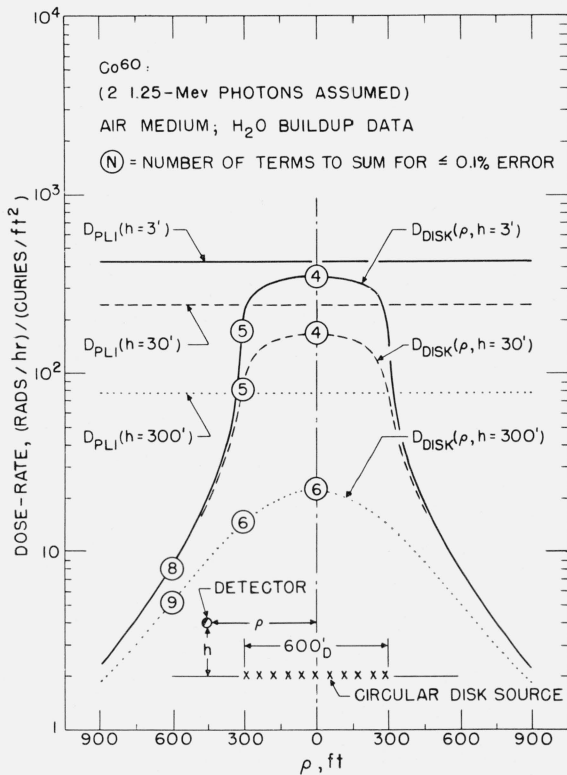
FIGURE 5. *Geometry and intermediate results for example 2.*

The solid, dashed and dotted horizontal lines are infinite-plane-source total dose-rates $D_{PLI}(h)$ calculated using (34) for detector heights $h=3$, 30, and 300 ft respectively. The corresponding total dose-rate profiles $D_{DISK}(\rho,h)$ over a 300-ft radius disk source were calculated using (19c).
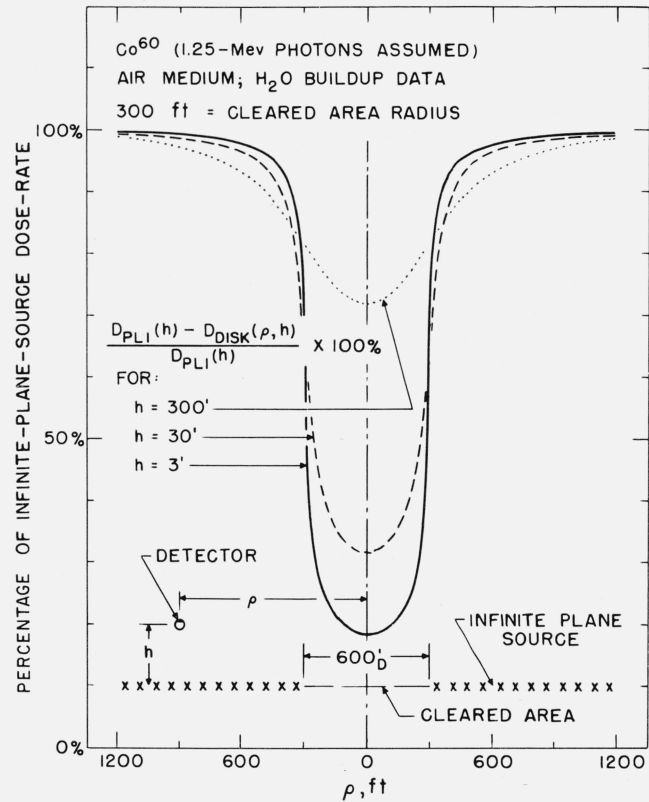
FIGURE 6. *Relative dose-rate profiles at heights 3, 30, and 300 ft above a 300-ft radius cleared circular area in an infinite plane Co–60 source in an infinite air medium (example 2).*

These profiles were obtained by subtracting the disk-source profiles $D_{DISK}(\rho,h)$ in figure 5 from the corresponding infinite plane source dose-rates $D_{PLI}(h)$, dividing by $D_{PLI}(h)$ and multiplying by 100 percent.

Caution must be taken in applying these results to the study of radiation fields from fallout deposition on the ground, since the ground-air interface has been shown by theoretical [36] and experimental [37, 38] studies to affect the scattered component by as much as a factor of three. Qualitatively, this would have the greatest effect on the $h=3$ ft profile in figure 5, "squaring the shoulders" of the curve and depressing the tails on either side. In figure 6 the 3-ft profile would more closely resemble a "square well," but the 30-ft and 300-ft profiles would not be appreciably changed.

8. Discussion

The power-series formulation for buildup data is seen to have two main limitations:

(a) Convergence of the primary-flux series (15), and hence the total-flux series (19), is poor for combinations of thick barriers ($\mu_0 x \gtrsim 1$) and detector-source separations much less than the source dimensions (i.e., a, $b \gg 1$ or $h \ll 1$). In such cases the geometry closely resembles the infinite plane source geometry for which the series (15) for $D°$ becomes, in the limit, the series representation ((5), [35]) for the exponential integral $E_1(\mu_0 x)$. The latter series converges absolutely for $0 < \mu_0 x < \infty$, but for $1 \lesssim$

$\mu_0 x < \infty$ the convergence rate is rather slow for practical use. In these situations it is more economical to revert to numerical integration, or to use an infinite plane source analytical formulation, such as (34) in example 2, as a close approximation.

(b) Boundary effects such as the density-interface effect [36–38] are neglected, but this limitation is inherent in any buildup factor formulation. Problems in which such effects are important are best treated by Monte Carlo techniques at present [36].

On the other hand, the series formulation provides some advantages:

(a) The three-way separation variables [(1) unique properties of the medium—$b_n(E_0, Z)$, (2) geometry—q_n (geom) and (3) barrier thickness—$\mu_0 x$] gives both economy of data tabulation and flexibility of application. A given set of buildup data can be applied to a variety of distributed source geometries, or vice versa, and at the same time the barrier thickness $\mu_0 x$ can be varied in a trivial fashion.

(b) In some simple idealized geometries the series (19) can provide exact answers, especially in the region of small barrier thickness ($\mu_0 x \lesssim 1$). These answers, in addition to available experimental data, can then be used to check the validity of simpler engineering-type approximate methods (e.g., [3]) in this region.

---

9. References

[1] L. V. Spencer, Structure shielding against fallout radiation from nuclear weapons, NBS Mono. 42 (June 1, 1962).

[2] C. Eisenhauer, An engineering method for calculating protection afforded by structures against fallout radiation (unpublished).

[3] F. G. Moote, Dose rates from rectangular plaques, Nucleonics **19**, No. 7, 102 (1961).

[4] U. Ya. Margulis and A. V. Khrustalev, On the spatial distribution of the gamma-ray dose from a plane source (Experimental data for rectangular Co–60 source; analysis in terms of inscribed and circumscribed circular sectors), At. Energ. **3**, 338 (1957); transl. in Int. J. Appl. Rad. and Isotopes **4**, 109 (1958).

[5] J. A. Auxier, J. O. Buchanan, C. Eisenhauer, and H. E. Menker, Experimental evaluation of the radiation protection afforded by residential structures against distributed sources, CEX–58.1, ORNL (Jan. 19, 1959), and C. Eisenhauer, Analysis of experiments on light residential structures with distributed Co–60 sources (unpublished NBS Report 6539, Oct. 15, 1959).

[6] R. M. Sievert, Die Intensitätsverteilung der primaren γ–Strahlung in der Nähe medizinischer Radiumpräparate, Acta Radiol. (Stockholm) **1**, 89 (1921).

[7] J. H. Hubbell, R. L. Bach, and J. C. Lamkin, Radiation field from a rectangular source, NBS J. Res. **64C**, (Eng. and Instr.) No. 2, 121 (1960).

[8] J. H. Hubbell, R. L. Bach, and R. J. Herbold, Radiation field from a circular disk source, NBS J. Res. **65C**, (Eng and Instr.) No. 4, 249 (1961).

[9] M. A. Capo, Polynomial approximation of gamma ray buildup factors for a point isotropic source, APEX–510 (Nov. 1958).

[10] J. H. Hubbell, Dose distribution from finite plane sources using point source buildup data (abstract), Radiation Res. **16**, 598 (1962).

[11] H. Goldstein, The attenuation of gamma rays and neutrons in reactor shields, eq (98), p. 187, USAEC (May 1, 1957).

[12] A. B. Chilton, D. Holoviak, and L. K. Donovan, Determination of parameters in an empirical function for build-up factors for various photon energies, U.S. Naval Civil Engineering Laboratory, Tech. Note N–389 (Aug. 1960).

[13] N. I. Leshchinskii, Method of calculating dosage field of powerful isotopic units, At. Energ. **8**, 62 (1960); transl. in Soviet J. At. Energy **8**, 59 (1961).

[14] J. J. Taylor, Application of gamma ray build-up data to shield design, WAPD–RM–217 (Jan. 21. 1954).

[15] M. J. Berger and L. V. Spencer, Penetration of gamma rays from isotropic sources through aluminum and concrete, NBS Tech. Note 11 (May 11, 1959).

[16] N. E. Taney, Preliminary considerations of the use of radioisotopes for laboratory tracer techniques, Ann. Bull. of the Beach Erosion Board **14**, 16 (1960). [Note: The word "Legendre" on page 23 of this reference should be changed to read "power series."]

[17] D. C. Brunton (proj. mgr.), Final report on the high intensity food irradiator, HIFI Rep. No. 17 (May 1, 1960).

[18] B. Manowitz, O. A. Kuhl, L. Galanter, R. H. Bretton, and S. Zwickler, Experimental parametric study of large-scale Co-60, Na–24 and Cs–137 slab irradiators, p. 65–91 of Large Radiation Sources in Industry, International Atomic Energy Agency, Vienna, 1960.

[19] W. V. Mayneord, The distribution of radiation around simple radioactive sources, Brit. J. Radiol. **5**, 677 (1932).

[20] J. P. Jain and B. L. Sharma, Effect of building-up factor on the optimum shape for a shielding barrier, Reactor Sci. and Technology **16**, 375 (1962).

[21] U. Fano, L. V. Spencer, and M. J. Berger, Penetration and Diffusion of X-rays, Encyclopedia of Physics **38**, II, p. 813 (Springer-Verlag, 1959).

[22] For precise definitions of "flux" and "current" see, for example, G. N. Whyte, Principles of Radiation Dosimetry, p. 3. (John Wiley & Sons, New York, N.Y., 1959). Note, however, that Whyte introduces the designations "spherical intensity", I_s, and "plane intensity," I_p, for flux and current, respectively.

[23] G. White Grodstein, X-ray attenuation coefficients from 10 kev to 100 Mev, NBS Circ. 583 (1957).

[24] R. T. Berger, The x- or gamma-ray energy absorption or transfer coefficient: Tabulations and discussion, Rad. Res. **15**, 1 (1961).

[25] This polynomial formulation was also suggested by L. V. Spencer as the basis for an unpublished report (J. H. Hubbell, Dose due to distributed gamma-ray sources) which contains parametric data for 0.255- to 3-Mev gamma rays in water.

[26] H. Goldstein and J. E. Wilkins, Jr., Calculations of the penetration of gamma rays, AEC NYO–3075 (1954).

[27] See, for example, U. Fano, C. D. Zerby, and M. J. Berger, Gamma-ray attenuation, ch. 10 of Reactor Handbook, III B: Shielding, p. 115, E. P. Blizard and L. S. Abbott, editors, (John Wiley & Sons, New York, N.Y. 1962).

[28] B. T. Price, C. C. Horton and K. T. Spinney, Radiation Shielding (Pergamon Press, New York, 1957); parameters for Al were supplied by J. R. A. Lakey.

[29] J. L. Meredith, Method of evaluation of experimental radiation measurements over a rectangular source, NDL–TR–11, April 1961.

[30] J. L. Donovan, Three-plaque, two-pass irradiator, Nucleonics **19**, No. 7, 104 (1961).

[31] Recommendations of the International Commission on Radiological Units, Radiology **62**, No. 1, 106 (1954).

[32] H. Mochizuki, Y. Tanaka, Y. Higashihara, K. Nagato, and K. Yorihisa, Experimental study on the penetra-

tion of Co–60 γ-ray through finite heterogeneous media, J. At. Energy Soc. Japan **4,** 448 (Part 1), 703 (Part 2) (1962).

[33] J. L. Donovan, private communication.

[34] E. T. Clarke and J. O. Buchanan, Radiation shielding against fallout, Nucleonics **20,** No. 8, 143 (1962).

[35] G. Placzek, The functions $E_n(x) = \int_1^\infty e^{-xu} u^{-n} du,$

MT–1, NRC No. 1547, Chalk River, Ont. (1946).

[36] M. J. Berger, Calculation of the energy dissipation by gamma radiation near the interface between two media, J. Appl. Phys. **28,** 1502 (1957).

[37] O. I. Leipunskii and V. N. Sakharov, Propagation of Co–60 radiation in the air above the earth, At. Energ. **6,** 585 (1959); transl. in Soviet J. At. Energy **6,** 440 (1960).

[38] C. E. Clifford, J. A. Carruthers and J. R. Cunningham, γ-radiation at air-ground interfaces with distributed Cs–137 sources, Can. J. Phys. **38,** 504 (1960).

(Paper 67C4–140)